



OPEN ACCESS

EDITED BY

Xiao-Feng Li,
Jinan University, China

REVIEWED BY

Dimitrios Vynios,
University of Patras, Greece
Orest William Blaschuk,
Zonula Inc., Canada

*CORRESPONDENCE

Hui Lu

✉ huilu@zju.edu.cn

Mengjie Dong

✉ dmjzf2016@zju.edu.cn

†These authors have contributed equally to this work

RECEIVED 18 December 2022

ACCEPTED 06 March 2023

PUBLISHED 22 May 2023

CITATION

Liu Z, Wen G, Huang Y, Dong Y, Wang Z, Alhaskawi A, Zhang S, Wang G, Ye Q, Zhou H, Lu H and Dong M (2023) [¹⁸F]AIF-NOTA-ADH-1: A new PET molecular radiotracer for imaging of N-cadherin-positive tumors.
Front. Oncol. 13:1126721.
doi: 10.3389/fonc.2023.1126721

COPYRIGHT

© 2023 Liu, Wen, Huang, Dong, Wang, Alhaskawi, Zhang, Wang, Ye, Zhou, Lu and Dong. This is an open-access article distributed under the terms of the [Creative Commons Attribution License \(CC BY\)](https://creativecommons.org/licenses/by/4.0/). The use, distribution or reproduction in other forums is permitted, provided the original author(s) and the copyright owner(s) are credited and that the original publication in this journal is cited, in accordance with accepted academic practice. No use, distribution or reproduction is permitted which does not comply with these terms.

[¹⁸F]AIF-NOTA-ADH-1: A new PET molecular radiotracer for imaging of N-cadherin-positive tumors

Zhenfeng Liu^{1†}, Guanghua Wen^{2†}, Yuqiao Huang³, Yanzhao Dong³, Zewei Wang⁴, Ahmad Alhaskawi⁵, Shuyi Zhang¹, Guolin Wang¹, Qianni Ye¹, Haiying Zhou⁵, Hui Lu^{5*} and Mengjie Dong^{1,6*}

¹Department of Nuclear Medicine, The First Affiliated Hospital, Zhejiang University School of Medicine, Hangzhou, China, ²Department of Nuclear Medicine, Shenzhen Longhua District Central Hospital, Shenzhen, China, ³Institute of Translational Medicine, Zhejiang University, Hangzhou, China, ⁴Department of Clinical Medicine, Zhejiang University School of Medicine, Hangzhou, China, ⁵Department of Orthopedics, The First Affiliated Hospital, Zhejiang University School of Medicine, Hangzhou, China, ⁶Department of Nuclear Medicine, Peking University Shenzhen Hospital, Shenzhen, China

Background: The cell adhesion molecule (CAM) N-cadherin has become an important target for tumor therapy. The N-cadherin antagonist, ADH-1, exerts significant antitumor activity against N-cadherin-expressing cancers.

Methods: In this study, [¹⁸F]AIF-NOTA-ADH-1 was radiosynthesized. An in vitro cell binding test was performed, and the biodistribution and micro-PET imaging of the probe targeting N-cadherin were also studied in vivo.

Results: Radiolabeling of ADH-1 with [¹⁸F]AIF achieved a yield of up to 30% (not decay-corrected) with a radiochemical purity of >97%. The cell uptake study showed that Cy3-ADH-1 binds to SW480 cells but weakly binds to BXP3 cells in the same concentration range. The biodistribution results demonstrated that [¹⁸F]AIF-NOTA-ADH-1 had a good tumor/muscle ratio (8.70±2.68) in patient-derived xenograft (PDX) tumor xenografts but a lower tumor/muscle ratio (1.91±0.69) in SW480 tumor xenografts and lowest tumor/muscle ratio (0.96±0.32) in BXP3 tumor xenografts at 1 h post-injection (p.i.) These findings were in accordance with the immunohistochemistry results. The micro PET imaging results revealed good [¹⁸F]AIF-NOTA-ADH-1 tumor uptake in pancreatic cancer PDX xenografts with strong positive N-cadherin expression, while lower tumor uptake in SW480 xenografts with positive expression of N-cadherin, and significantly lower tumor uptake in BXP3 xenografts with low expression of N-cadherin, which was consistent with the biodistribution and immunohistochemistry results. The N-cadherin-specific binding of [¹⁸F]AIF-NOTA-ADH-1 was further verified by a blocking experiment involving coinjection of a non radiolabeled ADH-1 peptide, resulting in a significant reduction in tumor uptake in PDX xenografts and SW480 tumor.

Conclusion: [¹⁸F]AIF-NOTA-ADH-1 was successfully radiosynthesized, and Cy3-ADH-1 showed favorable N-cadherin-specific targeting ability by in vitro data.

The biodistribution and microPET imaging of the probe further showed that [18F]AIF-NOTA-ADH-1 could discern different expressions of N-cadherin in tumors. Collectively, the findings demonstrated the potential of [18F]AIF-NOTA-ADH-1 as a PET imaging probe for non-invasive evaluation of the N-cadherin expression in tumors.

KEYWORDS

PET imaging probe, N-cadherin, [18 F]AIF-NOTA-ADH-1, cancer, EMT

1 Introduction

Tumor invasion and metastasis are the key processes in tumor deterioration and are associated with poor prognosis. In recent years, a growing number of studies have found that the metastasis of most tumors depends on the epithelial-mesenchymal transition (EMT) (1–4). EMT is a biological developmental process characterized by epithelial cells losing the epithelial features and acquiring mesenchymal properties (5). The process of EMT is accompanied by epithelial cadherin (E-cadherin) down-regulation and the concomitant up-regulation of neural cadherin (N-cadherin) (6–9). Transfection of N-cadherin into tumor cells with negative N-cadherin expression resulted in significantly higher aggressiveness, while the intercellular adhesion mediated by E-cadherin disappeared, and the expression of E-cadherin was significantly decreased (10, 11). N-cadherin is absent or has low expression in normal epithelial cells, and abnormal expression of N-cadherin has been associated with epithelial malignancies such as breast cancer, prostate cancer, and uroepithelial carcinoma (12, 13). Considering the high expression of N-cadherin in tumors, it can be an excellent target for tumor treatment and diagnosis. Controlling tumor metastasis and reducing drug resistance by inhibiting N-cadherin may be an effective treatment strategy (14, 15). The pentapeptide ADH-1 is an N-cadherin inhibitor (12, 16–19) that specifically binds to N-cadherin through hydrophobic and electrostatic interactions, involving the interaction between the Trp2 residue of the binding site of N-cadherin with the Ala fragment of the ADH-1 molecule (20). Applying ADH-1 to tumors can lead to tumor vascular angiolysis and apoptosis (21–23), but does not damage normal mature blood vessels (22, 23). A combination of ADH-1 and melphalan was explored in the treatment of melanoma in mice, which significantly reduced tumor growth. The effect was equivalent to 30 times the dose of melphalan alone (23). The enhanced response of ADH-1 to melphalan was associated with increased tumor cell apoptosis, increased DNA adduct formation, and altered intracellular signaling. Clinical experiments investigating ADH-1 (phase 1 and phase 2 single-agent studies) showed anti-cancer activity in patients with N-cadherin-positive tumors (17, 24).

As an emerging field, molecular imaging has attracted significant attention and developed quickly in recent years. The combination of small peptides or small molecules with positron

nuclide labeling can be used as new molecular probes for functional imaging (25). Developing a molecular probe targeting N-cadherin for noninvasive imaging of N-cadherin *in vivo* has potential application value in tumor diagnosis, drug development, dose optimization, and treatment monitoring. In this study, a novel PET probe [18F]AIF-NOTA-ADH-1 was prepared by using ADH-1 peptide, and the feasibility of [18F]AIF-NOTA-ADH-1 for the detection of N-cadherin positive tumors was explored.

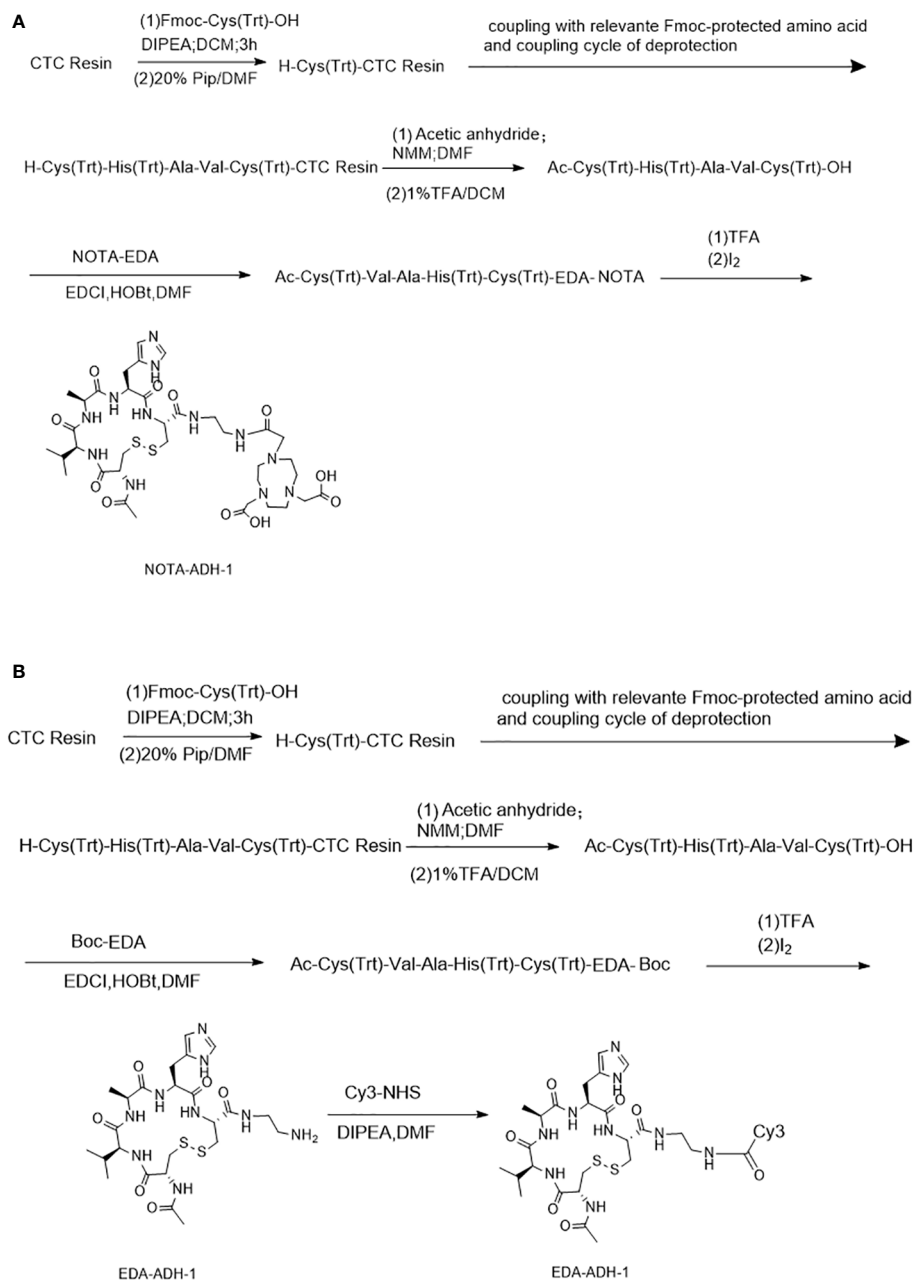
2 Materials and methods

2.1 General

The NOTA was purchased from Macrocyclic, Inc; protected amino acids, other peptide synthesis reagents, and resins were obtained from Nanchang tanzhenbio Co., Ltd; anhydrous aluminum chloride (AlCl₃) and sodium acetate were purchased from Alfa Aesar (China) Chemicals Co., Ltd; and trifluoroacetic acid (TFA) was obtained from Shanghai Aladdin Biochemical Technology Co., Ltd. (China). Reagents, including phosphate-buffered saline (PBS) and cell culture medium, were obtained from Sigma-Aldrich. Fetal bovine serum (FBS) was purchased from Biological Industries (BI) company. All reagents and solvents were commercial products and used without further purification. The Siemens Cyclotron produced [18F] fluoride by bombarding a [18O] H₂O target with 12.5 MeV protons. Analytical HPLC (high-performance liquid chromatography) was performed on an Agilent 1200 system with a reversed-phase column (Agilent Zorbax ODS, 250 × 4.6 mm). Mass spectra were obtained on a Q-T of a premier UPLC system equipped with an electrospray interface (ESI) (Waters, USA). A γ -counter (CAPRA-R, Capintec, Inc., Ramsey, New Jersey, USA) was used to measure the radiation value of the biological distribution experiment. Small animal imaging was performed using a micro-PET/CT scanner (Siemens Inveon Multimodality System, Germany).

2.2 Synthesis of peptides

Scheme 1 describes the peptides synthesized by the solid-phase synthesis method (26). The purity of the peptides, including



SCHEME 1

The synthesis process of the peptides of NOTA-ADH-1 (A) and Cy3-ADH-1 (B).

NOTA-ADH-1 and Cy3-ADH-1, was identified by high-performance liquid chromatography (HPLC), and the molecular weight was identified by mass spectrometry. They were stored at -20°C after freeze-drying.

2.3 Cell binding studies

Human colorectal carcinoma SW480 and pancreatic BxPC3 cell lines were purchased from the Institute of Biochemistry and Cell Biology, the Shanghai Institute for Biological Sciences, and the Chinese Academy of Sciences. Specific binding studies were

evaluated on SW480 and BxPC3 tumor cells. SW480 and BxPC3 cells were cultured in a medium containing high glucose and supplemented with fetal bovine serum, glutamine, and penicillin-streptomycin, and the culture medium was changed every other day. Cells were expanded in tissue culture pans in humidified air containing 5% carbon dioxide at 37°C and detached with trypsin and phosphate-buffered saline for further cell culture when cells were confluent.

To assess the binding ability of the peptide, the Cy3-ADH-1 peptide was synthesized. An equal number (1×10^5) of SW480 and BxPC3 cells were seeded in 6-well plates. After overnight incubation, 0.5 ml of culture medium and 0.5 ml of Cy3-ADH-1

solution with concentrations 5 μM , 20 μM , 50 μM , 100 μM , and 200 μM were added to the cell chambers in the dark, respectively, and incubated at 37°C in a 5% CO_2 incubator for half an hour. Subsequently, the solution in the 6-well plates was discarded, and the cells were fixed with paraformaldehyde for 10 min. After washing with PBS three times, the cells were mounted in a mounting medium containing DAPI for 15 minutes and then visualized by an Olympus IX71 fluorescence microscope (Olympus, Japan).

A competitive binding assay was performed on SW480 tumor cells. Therefore, 1×10^5 SW480 cells were placed in 3-well plates, and 0.5 ml of unlabeled ADH-1 solution of 0 μM , 50 μM , and 200 μM concentration were added to each well and incubated at 37°C in binding buffer. After 30 minutes of reaction, 0.5 ml of 10 μM Cy3-ADH-1 solution was added and then incubated in binding buffer at 37°C for another 1 hour to allow fluorescently-labeled polypeptides and excess non-labeled polypeptides to combine with tumor cells. The cells were then washed 3 times with 1ml PBS solution for 5 min each time and were mounted in a mounting medium containing DAPI for 15 minutes. The uptake intensity of SW480 colon cancer cells to fluorescently-labeled polypeptides was observed and measured by a fluorescence microscope.

2.4 Preparation of [^{18}F]AIF-NOTA-ADH-1

Scheme 2 describes the radiosynthesis routine of [^{18}F]AIF-NOTA-ADH-1 (27–31). 100 μg of NOTA-ADH-1 was dissolved in 2ml oxygen in a centrifuge tube with 400 μl pure water; AlCl_3 (26.0 nmol; 13.0 μL ; 2.0 mM) in sodium acetate buffer solution (pH 4; 0.2 M) and 1ml acetonitrile was added to the reactor and mixed well. 500 μl ^{18}F target water (1000-1500mCi) was added to the reactor and heated at 100°C for 10min; 5 μL of crude production point samples were collected for Thin-layer chromatography (TLC) detection. The remaining crude product was slightly cooled and then transferred to the pre-conditioned HLB cartridge with 15ml water and washed with 10ml PBS and 20ml water, respectively. The product was finally eluted with 2.0 mL of ethanol and water at a ratio of 1:1 (V/V), filtered using a sterile filtration membrane, and collected in the receiving bottle. The

product (310-500mCi) was then diluted into a solution containing 5% ethanol using normal saline for injection, and samples were taken for quality control.

2.5 Determination of radiochemical purity

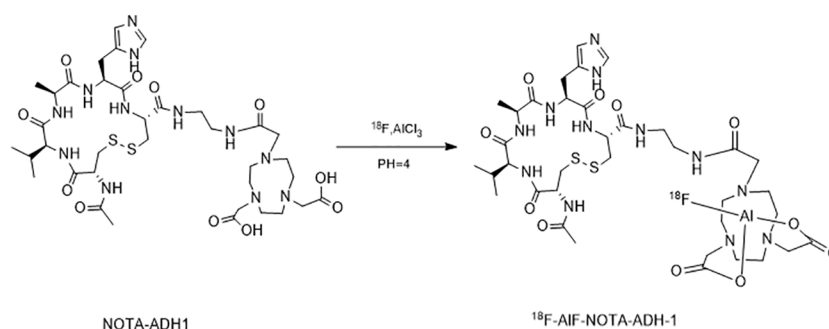
The radiochemical yield was monitored by TLC (50% acetonitrile), and the radiochemical purity was confirmed by HPLC using a Zorbax ODS(C18) 4.6 * 250 mm analysis column. The HPLC included the mobile phase A, a 0.1% acetonitrile solution of trifluoroacetic acid (TFA), and phase B, an aqueous solution of 0.1% TFA. The mobile phases were performed to carry out a gradient elution. The ratio of phase A to phase B at 0 min was 10%:90% and gradually rose to 70%:30% at 20 min, which was maintained at a flow rate of 1ml/min.

2.6 *In vitro* stability determination

The stability of [^{18}F]AIF-NOTA-ADH-1 was tested in PBS and bovine serum. In brief, 3.7 MBq of [^{18}F]AIF-NOTA-ADH-1 was pipetted into 0.5 mL of PBS and incubated in PBS at room temperature or bovine serum at 37°C. For the study, an aliquot of the solution was directly taken at 1, 6, and 8 h after incubation, and the radiochemical purity was determined by radio-TLC or radio-HPLC under identical conditions.

2.7 Lipid-water partition coefficient

The partition coefficient of [^{18}F]AIF-NOTA-ADH-1 was measured by assessing the distribution of radioactivity in 1-octanol and phosphate buffer in a 2 mL centrifuge tube. 20 μL of [^{18}F]AIF-NOTA-ADH-1 solution was added to a tube containing 0.5 mL each of 1-octanol and PBS. The mixture was vortexed and centrifuged (5,000 r/min) for 5 min. A total of 2 samples (50 μL) were collected from each layer and were assayed in a γ counter. Partition coefficients ($\log \text{Po/w}$) are shown as the log counts in 1-octanol vs. PBS layers (n=3).



SCHEME 2

The radiosynthesis routine of ^{18}F -AIF-NOTA-ADH-1.

2.8 Tumor implantation in mice

All animal experiments were performed in accordance with and approved by the Institutional Animal Care and Use Committee guidelines of the First Affiliated Hospital of Zhejiang University School of Medicine. BALB/c nu/nu mice (female, 20 ± 3 g, 4- to 6-week-old; Department of Laboratory Animal Science, Zhejiang University) were used in this study. The SW480 and BxPC3 xenografts were generated, and 5×10^6 tumor cells were subcutaneously injected into the flanks of female athymic nude mice. The PDX-bearing mouse models were established as follows. Pancreatic cancer (diagnosed as pancreatic ductal adenocarcinoma) tissues were obtained from the surgery of a 67-year-old female patient. Written informed consent was obtained from the patient, and the research protocol was approved by the Clinical Research Ethics Committee of the First Affiliated Hospital of Zhejiang University School of Medicine. The sample was sectioned into about 1mm^3 pieces, and the tumor tissues were subcutaneously implanted into BALB/c nu/nu mice flanks. Mice were allowed free access to sterile water and food and were kept under strict disease-free conditions with controlled temperature ($\sim 25^\circ\text{C}$), humidity (50-70%), and circadian rhythms (12-hour light/dark cycles). All necessary procedures were carried out to minimize discomfort and avoid the waste of animals. The length and width of the tumor were measured every other day. Biodistribution studies and positron emission tomography in mice were performed after the tumor volume reached 150 to 200mm^3 .

2.9 Biodistribution in normal mice

Thirty SPF Kunming mice weighing 18-20g were randomly divided into 6 groups ($n=5$). As described above, $[^{18}\text{F}]\text{AlF-NOTA-ADH-1}$ was purified and separated by HPLC analysis. Each mouse was injected with a dose of 0.74MBq ($20\mu\text{Ci}$) through a caudal vein. Blood was collected from the orbit, the mice were sacrificed, and the brain, heart, lung, liver, spleen, kidney, stomach, intestine, muscle, bone and other organs were taken at 2 min, 5 min, 15 min, 30 min, 60min and 120min after injection. The radioactivity results were recorded as injected radioactivity per gram of tissue (% ID/g) corrected for background and decay.

2.10 Biodistribution in the tumor xenograft model

The BALB/c nude mice were randomized into different tumor models (SW480, BxPC3, and pancreatic PDX), including 5 mice per group. Each nude mouse was injected with 0.74MBq ($20\mu\text{Ci}$) $[^{18}\text{F}]\text{AlF-NOTA-ADH-1}$ through the caudal vein. Blood was collected from the orbit, and the mice were dissected to collect the brain, heart, lung, liver, spleen, stomach, intestine, muscle, bone and others at 30 min, 30min, 60min, 90min and 120min after injection. In the blocked group, the study was performed with a saturating dose of ADH-1 (20 mg/kg of mouse body weight) intravenously

administered 60min before the intravenous injection of $[^{18}\text{F}]\text{AlF-NOTA-ADH-1}$ in the pancreatic PDX model and SW480 xenograft model. The mice in the tumor xenograft model were sacrificed 1h after $[^{18}\text{F}]\text{AlF-NOTA-ADH-1}$ injection. The nude mice were dissected, and tumor tissues and related tissues (blood, brain, heart, lung, liver, spleen, kidney, stomach, intestine, muscle and bone) were weighed, and their radioactivity was measured by γ -counter. The radioactivity results were recorded as % ID/g.

2.11 Micro-PET imaging

$[^{18}\text{F}]\text{AlF-NOTA-ADH-1}$ was evaluated by micro-PET imaging on nude mice bearing a PDX tumor, SW-480 and BxPC3 tumor xenografts. Each tumor-bearing nude mouse was injected with 3.7MBq $[^{18}\text{F}]\text{AlF-NOTA-ADH-1}$ *via* the tail vein. After being anesthetized with isoflurane, tumor-bearing nude mice were imaged using a micro-PET/CT scanner at 60 minutes post-injection under continuous isoflurane inhalation using a nasal mask with a connecting tube. Micro-PET/CT scanning was performed after low-dose 3D acquisition CT scanning at 10 minutes per bed. A blocking study was conducted, in which a saturating dose of unlabeled ADH-1 (20 mg/kg of mouse body weight) was intravenously administered 60 min before the intravenous injection of $[^{18}\text{F}]\text{AlF-NOTA-ADH-1}$.

The three-dimensional volume of interest (VOI) was used to assess the standard uptake value (SUV) of selected organs. The Seimens Inveon analysis software configured with micro-PET/CT was used to delineate the region of interest along the edge of the tumor and each normal tissue on the PET image. Subsequently, the SUV of each region of interest was measured, and the tumor/non-tumor ratio (T/NT) between the tumor and normal tissue was measured.

2.12 Immunohistostaining

Tumor tissues were fixed in 10% methanol for 4 hours. The samples were then dehydrated in graded ethanol, embedded in paraffin, and sliced into $5\mu\text{m}$ sections. Sections were incubated with N-cadherin (mouse monoclonal antibody, 1:200, Abcam) and then goat anti-mouse secondary antibodies (Abcam diluted 1:200). The secondary antibodies were formed by binding horseradish peroxidase (HRP) and Goat anti-mouse IgG. Then, the sections were stained with diaminobenzidine (DAB) staining solution. DAB generates brown precipitates under the catalysis of HRP, thereby amplifying signals and developing colors. After a series of routine processing, immunohistochemical images were finally obtained.

2.13 Statistical analysis

SPSS 26.0 software was used for analysis, and all quantitative data in the experiment were expressed as mean \pm SD. *t*-test analysis was used for the comparison of differences between two groups; analysis of variance was used for comparison between multiple

organizations. A *p*-value less than 0.05 was considered statistically significant.

3 Results

3.1 Synthesis of peptides

A standard Fmoc solid-phase synthesis was used to synthesize NOTA-ADH-1 and Cy3-ADH-1 (Scheme 1). The synthesized peptide was characterized by High Resolution Mass Spectrometry (HRMS) (Supplementary Figures S1, S2), and its purity was determined by HPLC, revealing a chemical purity of greater than 95%.

3.2 *In vitro* cell binding test

The *in vitro* results showed that the degree of SW480 cell uptake of Cy3-ADH-1 was concentration-dependent, exhibiting an increasing fluorescence intensity with increasing Cy3-ADH-1 concentration. In contrast, no obvious fluorescence signal was found in the blank control tube (Figure 1). Competitive inhibition assays demonstrated that unlabeled ADH-1 significantly affected the uptake of Cy3-ADH-1 in SW480 cells, with the 200nM inhibition group showing a substantially higher uptake than the 50nM inhibition group (Figure 2). No significant uptake (or fluorescence signal) of Cy3-ADH-1 by BXPC3 cells was observed in the concentration range of 5 μ M to 200 μ M (Figure 3).

3.3 Radiochemical synthesis

[¹⁸F]AIF-NOTA-ADH-1 was successfully prepared using the [¹⁸F]AIF method (Scheme 2). Thin-layer chromatography was performed on the reaction solution. As shown in Figure 4, the fluoride ion peak is at the origin, and the R_f of product [¹⁸F]AIF-NOTA-ADH-1 is 0.5. The non-decay corrected radiochemical yield of [¹⁸F]AIF-NOTA-ADH-1 was 28.07 \pm 2.42% (n=20), the radioactivity of the radiotracer was 310–500mCi, and HPLC analysis showed that the retention time of the drug was 9.4 min. The radio molar activity of the drug was 153.55 \pm 28.25 GBq/mmol, and the radiochemical purity was 98.1 \pm 0.6% (Figure 5). The total time of the radiosynthesis reaction was about 30 minutes. The [¹⁸F]AIF-NOTA-ADH-1 product was colorless and transparent, with a pH meter of 6.5. The drug is sterile, with bacterial endotoxin levels per 1mL less than 10 EU. The measured partition coefficient of the product was -2.45 \pm 0.09, indicating that the probe was hydrophilic. The drug was stable at 37 $^{\circ}$ C in PBS and calf serum, and the radiochemical purity was about 95.5 and 95.0%, respectively, after 8 h. The results indicated that [¹⁸F]AIF-NOTA-ADH-1 was stable *in vitro*.

3.4 Biological distribution of [¹⁸F]AIF-NOTA-ADH-1 in normal mice

The research results showed that [¹⁸F]AIF-NOTA-ADH-1 had rapid blood clearance. After injection of [¹⁸F]AIF-NOTA-ADH-1,

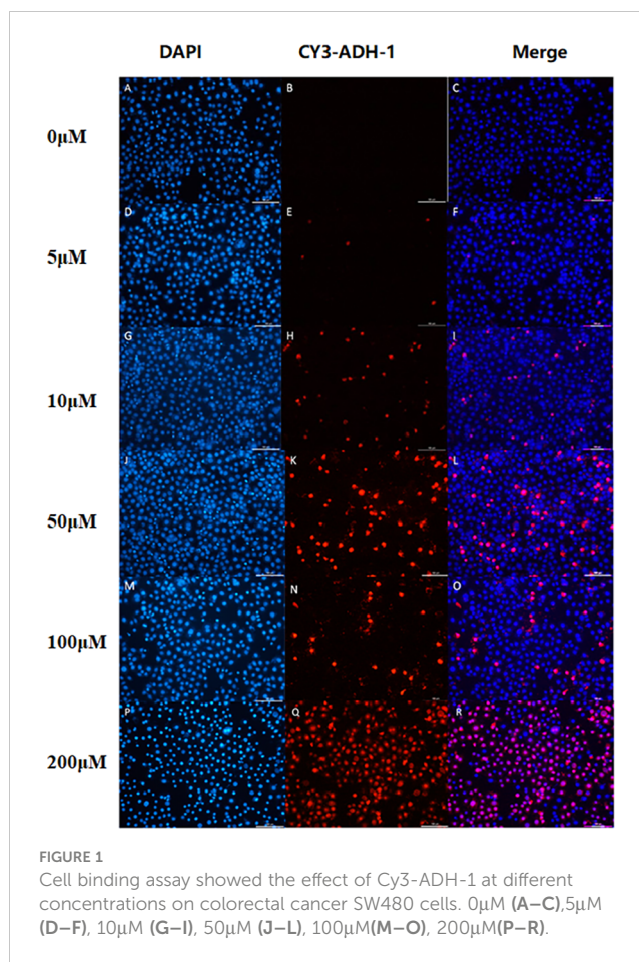


FIGURE 1
Cell binding assay showed the effect of Cy3-ADH-1 at different concentrations on colorectal cancer SW480 cells. 0 μ M (A–C), 5 μ M (D–F), 10 μ M (G–I), 50 μ M (J–L), 100 μ M (M–O), 200 μ M (P–R).

the radioactive concentration of [¹⁸F]AIF-NOTA-ADH-1 in blood was 18.84 \pm 1.95%ID/g at 2 min, 8.77 \pm 1.37%ID/g at 5 min, 3.79 \pm 1.19%ID/g at 15 min, and 2.28 \pm 0.81%ID/g at 30 min, which decreased significantly to 1.04 \pm 0.36%ID/g at 120min after injection. [¹⁸F]AIF-NOTA-ADH-1 is widely distributed in the kidney and the intestines, indicating that [¹⁸F]AIF-NOTA-ADH-1 is mainly excreted from the urinary system and hepatobiliary

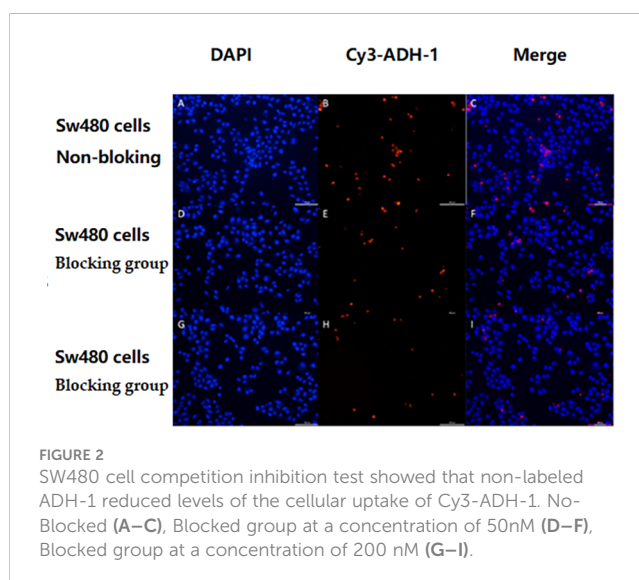
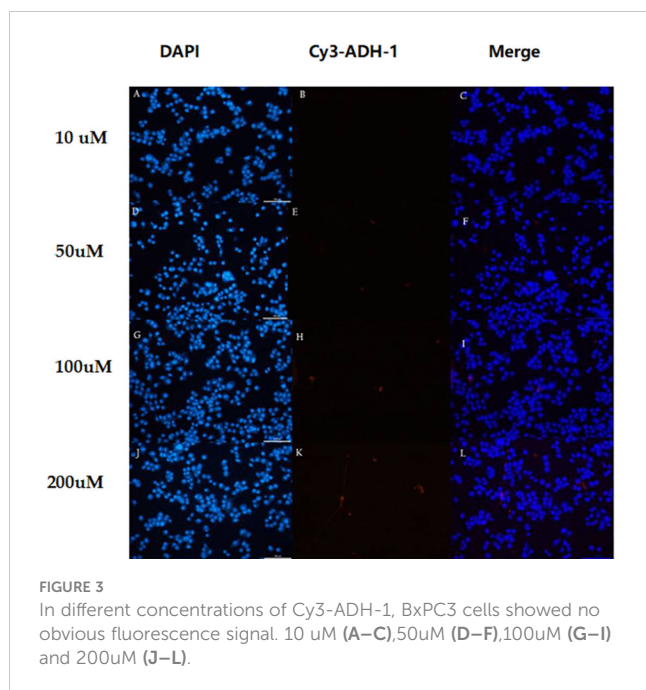


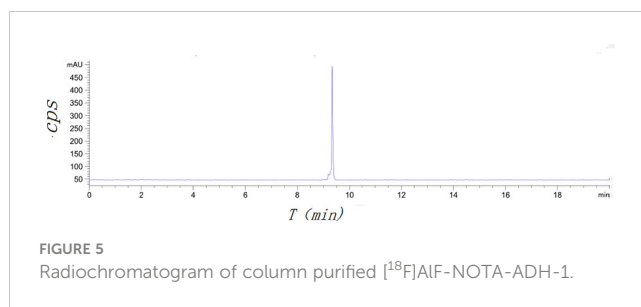
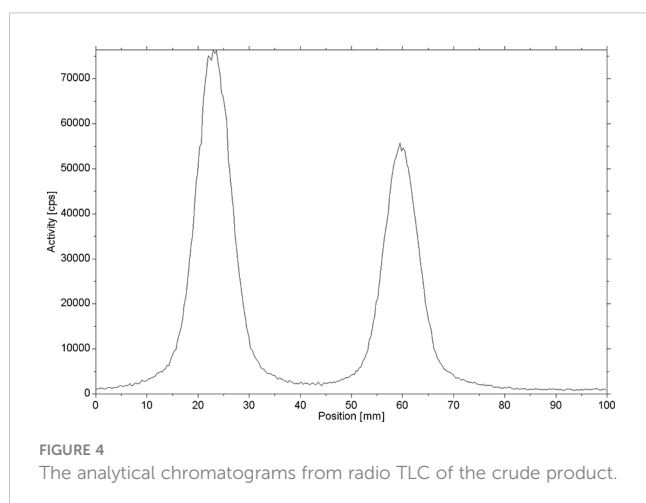
FIGURE 2
SW480 cell competition inhibition test showed that non-labeled ADH-1 reduced levels of the cellular uptake of Cy3-ADH-1. No-Blocked (A–C), Blocked group at a concentration of 50nM (D–F), Blocked group at a concentration of 200 nM (G–I).



systems. In addition, lower uptake was observed in the lungs, and muscle tissues and almost no uptake was seen in the brain tissue, suggesting that the probe does not efficiently cross the blood-brain barrier (Table 1).

3.5 Biological distribution of [¹⁸F]AIF-NOTA-ADH-1 in tumor-bearing nude mice

The biological distribution of normal tissues in tumor-bearing nude mice was similar to that of normal mice, with high radioactive uptake in the liver and kidneys (Tables 2–4). To investigate the tumor uptake of [¹⁸F]AIF-NOTA-ADH-1 in the pancreatic PDX xenograft model, tumors, blood, and tissue/organs were excised to measure the radioactivity. The highest tumor uptake was observed at 60 min after injection, suggesting that this may be an appropriate time for tumor imaging. In the blocking group, the radioactive



uptake of the tumor was $3.75 \pm 0.07\%$ ID/g at 60 min p.i, significantly lower than that in the non-blocking inhibition group ($t=5.304$, $p=0.006$). In SW480 tumor-bearing nude mice, the tumor/muscle (T/M) ratio was the highest at 60min (1.91 ± 0.69). In the blocking inhibition experiment, the radioactive uptake of the tumor was $1.07 \pm 0.57\%$ ID/g at 60min p.i, lower than that in the non-blocking group ($p=0.004$). In the BxPC3 tumor model, no significant uptake of [¹⁸F]AIF-NOTA-ADH-1 was observed in the tumor tissue.

3.6 In-vivo micro-PET imaging studies

Micro PET studies of [¹⁸F]AIF-NOTA-ADH-1 were performed on nude mice bearing pancreatic PDX, Human Colorectal Carcinoma SW480, and pancreatic BxPC3 tumor xenografts at 60 min p.i. A significantly increased radioactive uptake of tumor tissue was shown in the PDX tumor model, with a tumor/muscle ratio of 8.069 ± 2.832 . Unlabeled ADH-1 inhibitors can significantly reduce the T/NT ratios, with a T/Bone of 2.263 ± 0.465 , and a T/Lung of 5.062 ± 0.805 (Figure 6). The T/NT ratios showed significant differences between the non-blocked group and the blocked group, including T/Muscle ($p=0.003$), T/Bone ($p=0.023$), T/Kidney ($p=0.0001$), T/Liver ($p=0.002$), and T/Lung ($p=0.001$). Immunohistochemical staining showed strong positive N-cadherin expression in tumor tissue, supporting the high specificity of [¹⁸F]AIF-NOTA-ADH-1 binding to tumors expressing N-cadherin *in vivo*.

As shown in Figure 7, micro-PET imaging of the SW480 tumor-bearing nude mouse model 60 min after injecting [¹⁸F]AIF-NOTA-ADH-1 revealed high radioactive uptake in the tumor with a tumor/muscle ratio of 1.443 ± 0.121 , T/Bone of 1.903 ± 0.273 , and T/Lung of 3.359 ± 2.998 , unlabeled ADH-1 inhibitors can significantly reduce the T/NT ratios, too. A significant difference in T/NT ratios was observed between the non-blocked group and the blocked group, including T/Muscle ($p=0.019$), T/Bone ($p=0.002$), T/Liver ($p=0.001$), and T/Lung ($p=0.008$). Immunohistochemical staining showed positive N-cadherin expression in the tumor tissue. However, no significant increase in radioactive uptake was observed in the tumor tissues of BxPC3-bearing tumor model mice, with a tumor/muscle ratio of 1.018 ± 0.498 , T/Bone 0.055 ± 0.022 , and T/lung 0.291 ± 0.195 . Immunohistochemical staining of N-cadherin showed low expression in tumor tissues (Figure 8).

TABLE 1 Biological distribution of [¹⁸F]AIF-NOTA-ADH-1 in normal mice($\bar{x} \pm SD$, %ID/g).

Organs	2min	5min	15min	30min	60min	120min
Brain	1.05±0.25	0.87±0.30	0.46±0.10	0.39±0.10	0.22±0.05	0.58±0.68
Heart	9.15±0.91	7.54±2.08	3.57±0.82	3.64±0.66	1.19±0.70	1.01±0.15
Lung	6.26±1.29	4.74±1.69	3.05±0.40	2.15±0.27	2.19±0.42	1.62±0.35
Liver	8.01±1.26	7.09±2.03	14.76±1.11	16.14±2.34	21.62±3.53	13.73±2.35
Spleen	3.84±1.47	5.09±1.29	3.08±0.55	2.66±0.22	1.81±0.57	1.24±0.30
Kidney	24.92±1.12	36.52±2.00	22.06±1.43	25.74±1.17	22.20±1.92	15.18±0.96
Stomach	5.63±1.98	7.27±1.89	4.26±0.55	4.78±0.98	2.32±0.56	1.55±0.20
Intestines	5.39±0.84	6.06±1.42	5.73±0.64	6.28±0.59	5.27±1.09	4.18±0.53
Muscle	3.97±0.56	5.91±1.16	2.79±0.68	3.32±1.77	1.08±0.21	1.22±0.70
Bone	5.30±0.94	6.71±0.62	3.72±0.29	3.09±0.26	1.51±0.36	1.38±0.73
Skin	5.60±0.85	5.08±2.74	3.11±1.47	2.59±0.96	1.85±1.48	1.10±0.96
Blood	18.84±1.95	8.77±1.37	3.79±1.19	2.28±0.81	2.15±0.18	1.04±0.36

4 Discussion

Recent studies have found that the loss of E-cadherin expression in some tumors is often accompanied by the up-regulation of N-cadherin expression (32, 33), which is also known as “the cadherin switch” (33, 34). N-cadherin molecule, also known as neural cadherin, has a molecular weight of 140KD and is mainly expressed in mesenchymal cells, endothelial cells, muscle cells, and hematopoietic stem cells (11). However, recent studies have

investigated the up-regulation of N-cadherin in a variety of tumors and its correlation with enhanced tumor invasiveness. In breast cancer, N-cadherin interacts with fibroblast growth factor receptor (FGFR) (35), activates signal pathways, and induces the expression of matrix metalloproteinase-9 (MMP-9) (36), thereby promoting tumor invasion and metastasis (20, 35). In bladder cancer, malignant melanoma, and prostate cancer, N-cadherin promotes tumor cell invasion by activating signaling pathways and inhibits tumor cell apoptosis, which is conducive to tumor cell survival (37,

TABLE 2 The biodistribution of [¹⁸F]AIF-NOTA-ADH-1 in PDX xenograft model($\bar{x} \pm SD$, %ID/g).

Organs	Non-blocking group				Blocking group
	30min	60min	90min	120min	60min
Blood	0.69±0.22	0.40±0.18	0.39±0.11	0.41±0.07	0.35±0.14
Brain	0.62±0.14	0.99±0.47	0.63±0.18	0.51±0.27	0.86±0.21
Heart	2.54±0.97	0.96±0.17	0.95±0.25	0.81±0.28	0.82±0.02
Lung	4.38±1.33	3.41±0.44	3.52±1.76	2.07±0.94	2.37±0.14
Liver	12.28±1.23	11.31±2.30	10.43±1.97	9.20±1.66	10.35±1.15
Spleen	1.81±0.48	1.41±0.24	1.13±0.03	0.86±0.25	1.25±0.20
Kidney	17.75±5.89	15.82±1.17	12.50±0.89	8.52±2.09	11.62±2.40
Stomach	3.23±1.69	3.40±0.12	6.16±1.58	1.60±1.04	2.24±0.16
Intestines	3.82±0.12	2.14±0.04	3.93±2.67	2.53±2.00	2.49±0.33
Muscle	1.41±0.20	1.56±0.07	2.03±0.05	1.18±0.60	1.68±0.06
Bone	1.74±0.81	2.29±0.96	1.65±1.30	0.74±0.35	2.16±0.09
Skin	0.11±0.04	0.95±0.46	1.51±0.02	1.56±0.66	0.54±0.14
Tumor	8.04±1.82	10.76±2.16	7.18±0.53	4.93±1.65	3.75±0.07
T/Blood	10.72± 1.02	19.21± 2.20	13.54± 0.35	10.27±1.36	9.39± 0.10
T/Muscle	5.69±0.72	8.70±2.68	4.15±1.86	3.97±1.56	2.12±0.06

TABLE 3 The biodistribution of [¹⁸F]AIF-NOTA-ADH-1 in SW480 xenograft model($\bar{x} \pm SD$, %ID/g).

Organs	Non-blocking group				Blocking group 60min
	30min	60min	90min	120min	
Blood	0.30±0.15	0.28±0.06	0.08±0.01	0.12±0.04	0.27±0.09
Brain	0.18±0.05	0.23±0.14	0.19±0.05	0.39±0.24	0.20±0.11
Heart	1.09±0.12	0.67±0.15	0.48±0.08	0.55±0.12	0.59±0.07
Lung	2.58±0.28	1.96±0.56	1.55±0.76	2.34±0.37	1.58±0.45
Liver	8.37±0.87	8.31±3.19	9.32±0.78	8.65±1.56	5.32±1.65
Spleen	0.86±0.26	0.82±0.38	0.71±0.23	0.71±0.15	0.88±0.33
Kidney	8.81±1.80	10.27±3.47	5.73±0.80	5.53±0.91	6.54±2.20
Stomach	5.53±2.81	7.07±0.55	3.13±1.66	1.24±0.01	5.19±1.01
Intestines	1.60±0.78	3.84±2.01	1.87±0.71	1.57±0.97	2.53±0.72
Muscle	0.99±0.19	1.99±1.02	0.78±0.30	0.85±0.14	1.59±0.87
Bone	1.24±0.16	1.63±0.39	0.64±0.17	0.86±0.06	0.84±0.21
Skin	1.01±0.56	1.23±0.37	1.03±0.16	0.95±0.15	1.30±0.29
Tumor	1.73±0.11	2.08±1.64	0.96±0.15	0.73±0.67	1.07±0.57
T/Blood	5.77±0.13	7.42±1.01	9.6±0.76	6.08±0.35	3.96±0.33
T/Muscle	1.75±0.47	1.91±0.69	1.23±0.92	0.86±0.23	1.03±0.56

38). These studies suggest that N-cadherin can not only directly induce cell migration but also promote the survival of tumor cells and facilitate tumor cell invasion. In addition, studies have also shown that N-cadherin-mediated adhesion between tumor cells and mesenchymal cells plays an important role in the process of tumor

dissemination and metastasis (34). For example, in the invasive growth of melanoma (39), N-cadherin mediates the interaction between tumor cells and other cells in the dermis. It promotes fibroblasts to form extracellular matrix scaffolds and secrete cytokines and proteases by a paracrine mechanism (40). N-

TABLE 4 The biodistribution of [¹⁸F]AIF-NOTA-ADH-1 in BxPC3 xenograft models($\bar{x} \pm SD$, %ID/g).

Organ	30min	60min	90min	120min
Blood	0.25±0.05	0.18±0.11	0.09±0.06	0.25±0.19
Brain	0.95±0.61	1.71±0.05	0.49±0.02	0.43±0.29
Heart	1.93±0.46	3.83±0.29	1.70±0.28	1.04±0.06
Lung	2.60±0.23	1.95±0.12	1.06±0.14	0.86±0.56
Liver	6.80±1.65	8.53±1.69	6.73±1.20	5.25±1.51
Pancreas	0.23±0.08	0.61±0.09	0.49±0.23	0.65±0.11
Kidney	9.33±0.73	10.24±0.47	9.39±0.75	6.61±0.87
Stomach	3.12±0.36	2.96±0.42	2.14±0.22	1.78±0.19
Intestines	1.52±0.39	3.55±0.29	0.44±0.21	0.52±0.08
Muscle	1.03±0.40	1.05±0.58	0.91±0.08	0.58±0.28
Bone	2.17±0.19	3.45±0.10	1.90±0.11	1.69±0.39
Skin	3.00±0.74	3.31±0.43	1.23±0.14	0.84±0.19
Tumor	0.89±0.12	1.07±0.36	0.60±0.12	0.37±0.07
T/Blood	3.18±0.08	4.22±0.23	5.45±0.10	1.42±0.13
T/Muscle	0.86±0.21	0.96±0.32	0.66±0.19	0.63±0.23

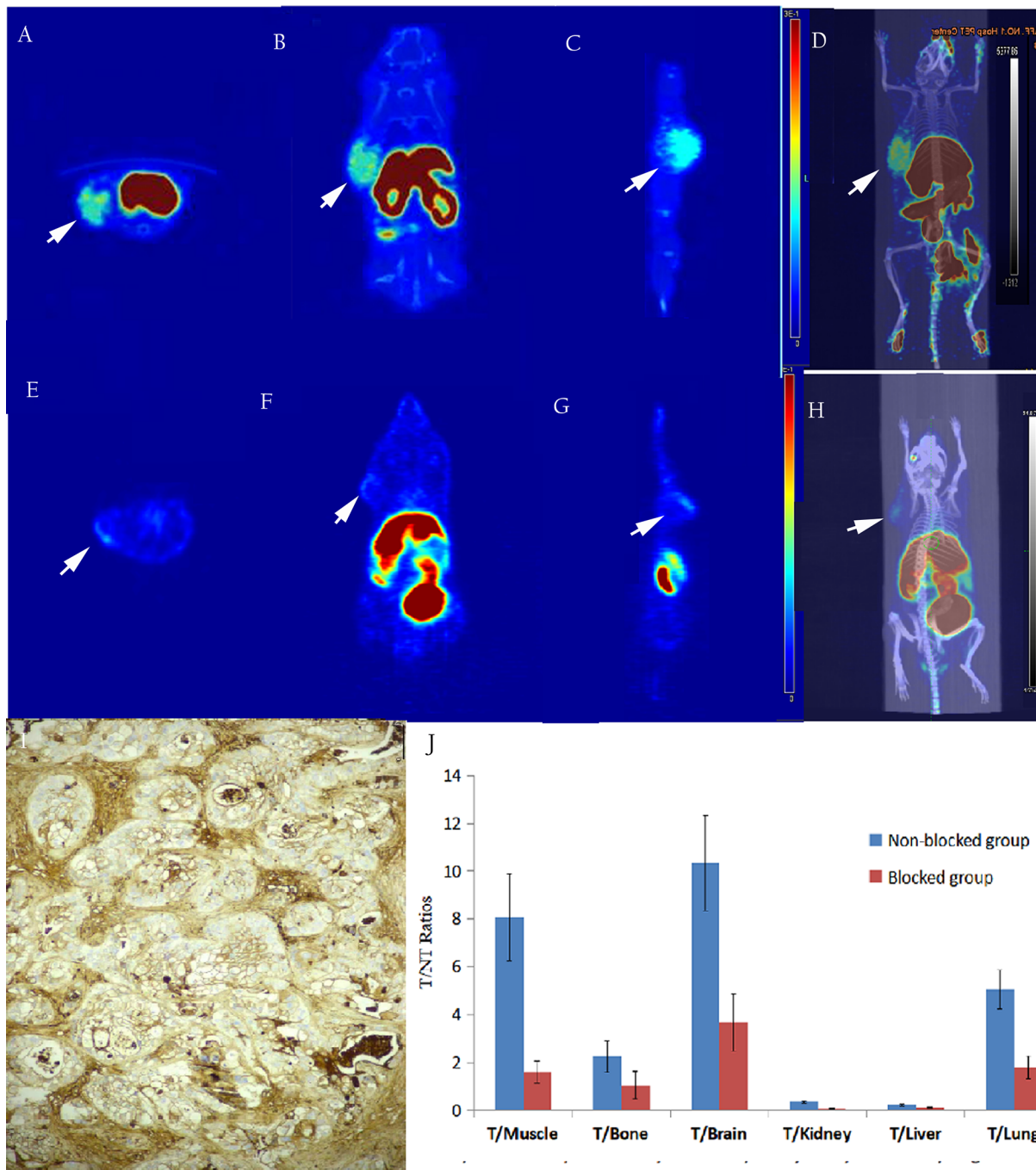


FIGURE 6 The *in-vivo* micro-PET/CT imaging of subcutaneous pancreatic PDX xenograft model at 60 min after injection of [¹⁸F]AIF-NOTA-ADH-1, high radioactive uptake of tumor tissue in the unblocked group (A–D) and significantly decreased in the blocked group (E–H). Immunohistochemical staining showed a significantly higher expression of N-cadherin (I×400); T/NT ratios in the unblocked group and blocked group (J).

cadherin also plays an essential role in angiogenesis and maturation. Blocking the function of N-cadherin by inhibitory antibodies during embryonic development led to the defect of pericyte recruitment and interfered with angiogenesis (41).

Therefore, N-cadherin can promote tumor invasion and metastasis by inducing cell migration, inhibiting apoptosis, mediating adhesion between tumor cells and mesenchymal cells, and promoting angiogenesis (22). Therefore, N-cadherin could be

used as a new target for tumor diagnosis and treatment. ADH-1 is the main N-cadherin antagonist, which significantly alters N-cadherin adhesion, proliferation, and migration, as well as enhancing cell apoptosis in many tumors (11, 18, 42). The phase 1 clinical study involving sixteen human patients with metastatic melanoma, including six patients who had not responded to melphalan alone, revealed that treatment with ADH-1 plus melphalan was effective. Within three months of treatment, eight

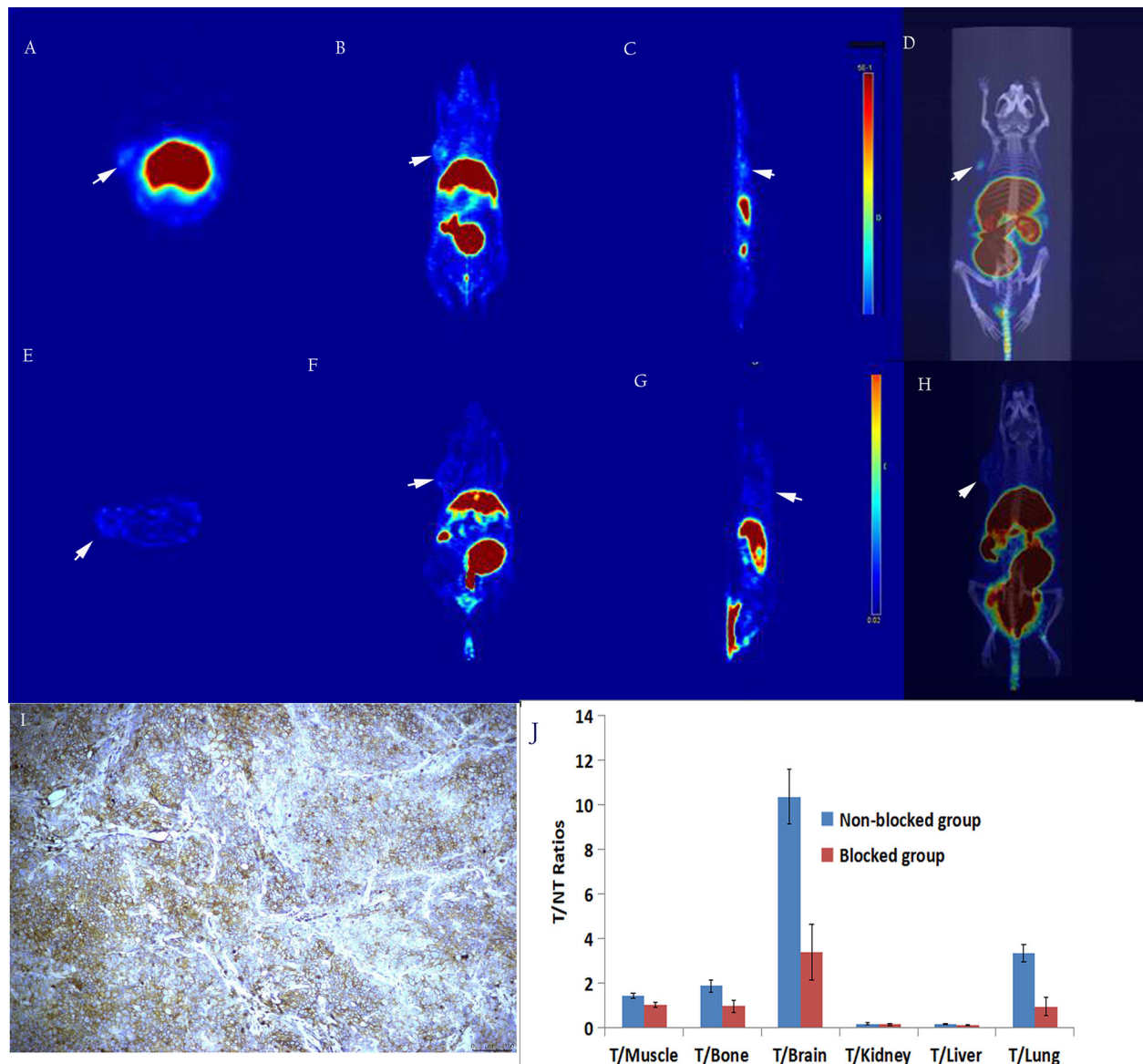


FIGURE 7

In vivo micro-PET/CT imaging of the subcutaneous SW480 xenograft model suggested that the radioactive uptake of the tumor tissue in the unblocked group (A–D) was significantly decreased in the blocked group (E–H). Immunohistochemical staining showed a high expression of N-cadherin (I, $\times 200$); T/NT ratios in the unblocked group and blocked group (J).

patients showed a complete response, two had a partial response, two had stable disease, and four had progressive disease (23). Another phase I clinical study showed that the stable period of two patients with ovarian cancer was prolonged (17). However, as a targeted tumor therapy, ADH-1 actually benefits a small number of patients due to the biological heterogeneity of tumors. PET imaging can be used to identify tumor types, screen the patient population that could benefit from targeted therapy, evaluate the treatment response, and predict the treatment effect. In this study, the [^{18}F] AIF-labeled ADH-1 probe was radiosynthesized for N-cadherin specific-targeting imaging.

Cy3-labeled ADH-1 and the labeled precursor NOTA-ADH-1 were synthesized by the Fmoc method, and the immunofluorescence (IF) staining technique was used to research

the cellular uptake of compounds as well as the inhibition test. In addition, Cy3-ADH-1 could bind to SW480 cells at 5 μM , and orange fluorescence was detected at the membrane and in the cytoplasm. The quantity and intensity of tumor cell uptake increased with increasing concentration of Cy3-ADH-1 and reached the highest peak at 50 μM , and then remained constant with the increase of concentration. In contrast, the blank control tube showed no orange fluorescence. Simultaneous inhibition assays showed that SW480 cells were significantly blocked by excess unlabeled ADH-1. The inhibitory effect of 200 nM was better than that of 50 nM excess unlabeled ADH-1. This is in accordance with the receptor-ligand competition binding law. However, the pancreatic cancer BxPC3 cells showed no significant increase in fluorescence uptake in tumor tissues at different

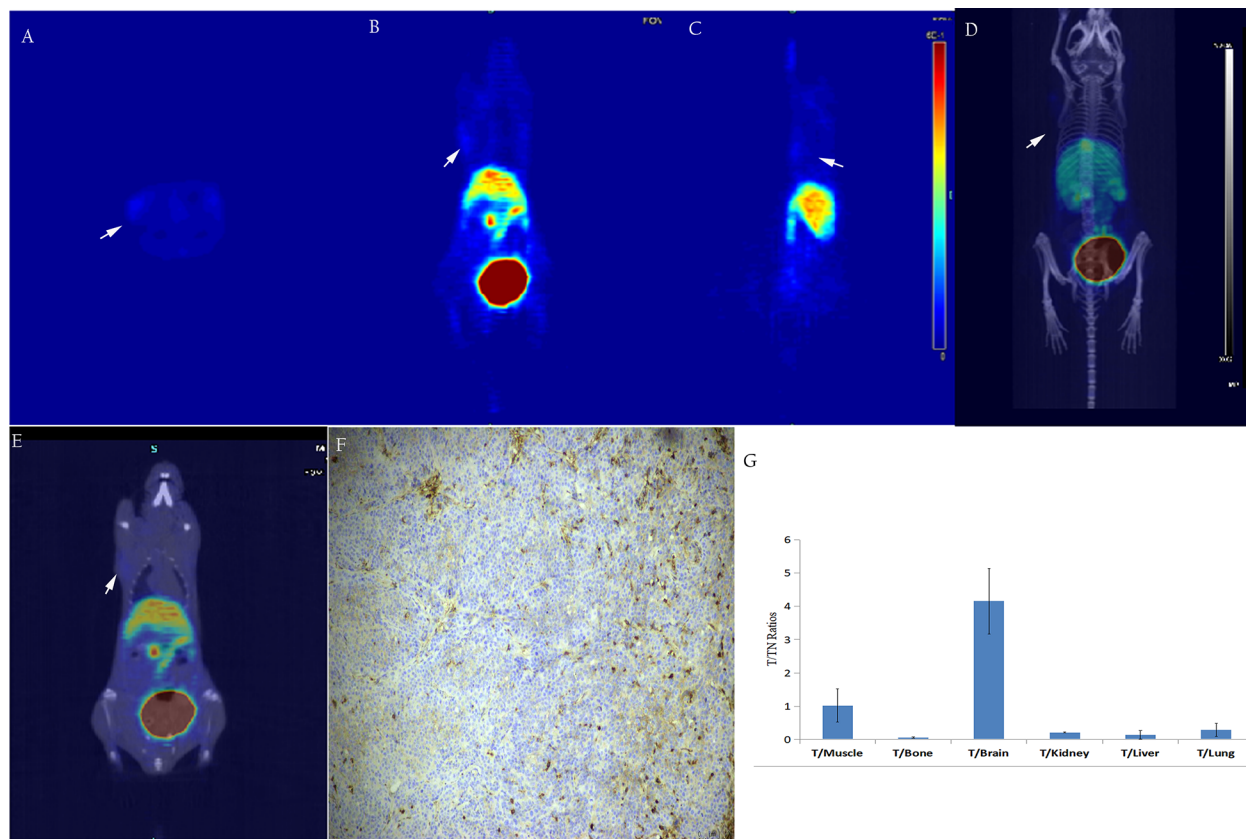


FIGURE 8

In vivo, micro-PET/CT imaging of the subcutaneous BxPC3 xenotransplantation model showed no significant increase in radiation uptake in tumor tissues (A–E). Immunohistochemical staining of N-cadherin in tumor tissue showed low expression in tumor tissue (F, $\times 200$); T/NT ratios (G).

concentration intervals from 5 μM to 200 μM , presumably due to the low N-cadherin expression in pancreatic cancer BxPC3 cells, which was confirmed by *in vivo* N-cadherin immunohistochemical staining in nude mice.

^{18}F was produced by cyclotron acceleration with a high yield (more than 1000mCi), and a half-life is 110 minutes. Compared with ^{68}Ga , ^{18}F can meet the inspection needs of a large number of patients; it is the ideal positron nuclide for labeling polypeptides (43). In this study, the [^{18}F]AIF labeling method was adopted (44, 45). In the incorporation reaction of ^{18}F Al and NOTA-ADH-1, the molar ratio of precursor to AlCl_3 is crucial. The labeling yield was the highest (55%) at an AlCl_3 concentration of 26 nmol and 5.5 times precursor. However, excessive AlCl_3 results in decreased labeling yields as Al can form a stable complex with NOTA, competing with ^{18}F Al chelation, resulting in a lower labeling rate. Compared with the C-18 column, the yield with the HLB column was higher, and ^{18}F ions with high polarity and polar buffer solution could be removed. The radiochemical purity of the obtained product was very high, requiring no further HPLC purification to meet clinical needs. Furthermore, the labeled product was stable in serum, and *in vivo* biodistribution experiments confirmed that the bone uptake was not high, indicating no obvious *in vivo* defluorination.

In order to study the targeting effect of the probe, mice bearing tumors with different expressions of N-cadherin were selected for the study. The biodistribution showed that the probe largely

accumulated in the kidneys and livers and subsequently attenuated over time, suggesting excretion mainly through the renal urinary and hepatobiliary systems. The biodistribution results of [^{18}F]AIF-NOTA-ADH-1 in the mice bearing pancreatic cancer PDX tumor showed that the probe accumulated more prominently in the tumor, with the highest tumor/non-tumor tissue ratio at 60 min, which was related to the high expression of N-cadherin. The biodistribution in SW480 tumor-bearing nude mice revealed mild uptake of the probe, with the peak tumor/muscle ratio at 60 min, which gradually decreased with time. The mild uptake was also correlated with the moderate staining of N-cadherin expression in the immunohistochemical staining of pathological tissues. In pancreatic cancer BxPC3 tumor-bearing nude mice, the tumor/muscle ratio was lowest, which was consistent with the low expression of N-cad in this tumor type. The biodistribution in different tumors illustrates that the probe is specifically associated with N-cadherin expression in tumor tissue.

In addition, in order to study whether there is competitive inhibition in the tumor tissue, 20 mg/kg of unlabeled ADH-1 solution was co-injected as the block group in the PDX tumor, and the radioactive uptake value of the tumor was significantly lower than that of the non-blocking inhibition group, which was $3.75 \pm 0.07\%$ ID/g and $10.76 \pm 2.16\%$ ID/g 60 minutes after injection, respectively ($p=0.006$). In the SW480 tumor, the radioactive uptake value was also lower than in the non-blocking

inhibition group. Blocking experiments in PDX and SW480 tumor models indicated that [^{18}F]AIF-NOTA-ADH-1 has good targeting specificity.

Micro PET/CT imaging of the pancreatic cancer PDX model showed good tumor uptake 60 minutes after injection, with the tumor/muscle ratio reaching 8.70 ± 2.68 . Moreover, PDX tumor-blocking experiments showed that tumors could be blocked by a nonradioactive ADH-1 small peptide and attenuated by imaging, which concurred with the biodistribution experiments in the PDX model. The nude mouse model of SW480 demonstrated mild tumor uptake, and SW480 tumors could also be blocked by a nonradioactive ADH-1 small peptide and attenuated by imaging. PET imaging of the BxPC3 pancreatic cancer models showed minimal tumor uptake, and immunohistochemical experiments showed strongly positive N-cadherin expression in PDX tumors, positive expression in SW480 tumors, and low expression in BxPC3 tumors. The micro-PET results showed that the probe [^{18}F]AIF-NOTA-ADH-1 could discern the expression of N-cadherin in tumors.

5 Conclusions

In the present study, the N-cadherin-targeted fluorescent and NOTA-modified derivatives Cy3-ADH-1 and NOTA-ADH-1 were successfully synthesized. The N-cadherin-targeted PET imaging probe [^{18}F]AIF-NOTA-ADH-1 was successfully radiosynthesized. Fluorescence imaging showed that Cy3-ADH-1 could be absorbed by SW480 cells, and its uptake was inhibited by excessive ADH-1, whereas pancreatic cancer BxPC3 cells showed no significant uptake of the fluorescent probe Cy3-ADH-1. *In vivo* biodistribution studies and micro-PET/CT imaging studies of [^{18}F]AIF-NOTA-ADH-1 confirmed that the PET imaging probe could distinguish between tumors with different expressions of N-cadherin. Blocking experiments showed that tumors could be blocked by a nonradioactive ADH-1 peptide in PDX and SW480 tumors, suggesting that [^{18}F]AIF-NOTA-ADH-1 has the specificity of N-cadherin and the probe had the potential for clinical transformation.

Data availability statement

The original contributions presented in the study are included in the article/Supplementary Material. Further inquiries can be directed to the corresponding authors.

Ethics statement

The studies involving human participants were reviewed and approved by ethics committee of the First Affiliated Hospital,

College of Medicine, Zhejiang University. The patients/participants provided their written informed consent to participate in this study. The animal study was reviewed and approved by Animal Experimental Ethics Committee of the first affiliated hospital, College of Medicine, Zhejiang University.

Author contributions

M-JD and HL designed the study. Z-FL and Y-QH radiosynthesized the probes and performed Micro-PET imaging. G-HW did cell study *in vitro*. YD, ZW performed data collection. AA, S-YZ, and G-LW analyzed the results. Q-NY and HZ drafted the manuscript. All authors contributed to the article and approved the submitted version.

Funding

This project was supported by the National Natural Science Foundation of China (Grant No. 81771884), Zhejiang Natural Science Foundation (LTGY23H180014) and Shenzhen Municipal Natural Science Foundation (JCYJ20220530160213030). The funding body only provided financial support, and the design of the study, analysis, and interpretation of data and the article writing were independently completed by the authors of this article.

Conflict of interest

The authors declare that the research was conducted in the absence of any commercial or financial relationships that could be construed as a potential conflict of interest.

Publisher's note

All claims expressed in this article are solely those of the authors and do not necessarily represent those of their affiliated organizations, or those of the publisher, the editors and the reviewers. Any product that may be evaluated in this article, or claim that may be made by its manufacturer, is not guaranteed or endorsed by the publisher.

Supplementary material

The Supplementary Material for this article can be found online at: <https://www.frontiersin.org/articles/10.3389/fonc.2023.1126721/full#supplementary-material>

References

- Dongre A, Weinberg RA. New insights into the mechanisms of epithelial-mesenchymal transition and implications for cancer. *Nat Rev Mol Cell Biol* (2019) 20(2):69–84. doi: 10.1038/s41580-018-0080-4
- Mittal V. Epithelial mesenchymal transition in tumor metastasis. *Annu Rev Pathol* (2018) 13:395–412. doi: 10.1146/annurev-pathol-020117-043854
- Lamouille S, Xu J, Derynck R. Molecular mechanisms of epithelial-mesenchymal transition. *Nat Rev Mol Cell Biol* (2014) 15(3):178–96. doi: 10.1038/nrm3758
- Basu S, Cheriyaundath S, Ben-Ze'ev A. Cell-cell adhesion: Linking wnt/ β -catenin signaling with partial EMT and stemness traits in tumorigenesis. *F1000Res*. (2018) 18(7):F1000Res. doi: 10.12688/f1000research.15782.1
- Kalluri R, Weinberg RA. The basics of epithelial-mesenchymal transition. *J Clin Invest* (2009) 119(6):1420–8. doi: 10.1172/JCI39104
- Wong SHM, Fang CM, Chuah LH, Leong CO, Ngai SC. E-cadherin: Its dysregulation in carcinogenesis and clinical implications. *Crit Rev Oncol Hematol* (2018) 121:11–22. doi: 10.1016/j.critrevonc.2017.11.010
- Muramaki M, Miyake H, Terakawa T, Kusuda Y, Fujisawa M. Expression profile of e-cadherin and n-cadherin in urothelial carcinoma of the upper urinary tract is associated with disease recurrence in patients undergoing nephroureterectomy. *Urology* (2011) 78(6):1443.e7–12. doi: 10.1016/j.urol.2011.07.1388
- Seo DD, Lee HC, Kim HJ, Min HJ, Kim KM, Lim YS, et al. Neural cadherin overexpression is a predictive marker for early postoperative recurrence in hepatocellular carcinoma patients. *J Gastroenterol Hepatol* (2008) 23(7 Pt 1):1112–8. doi: 10.1111/j.1440-1746.2007.05182.x
- van Roy F. Beyond e-cadherin: roles of other cadherin superfamily members in cancer. *Nat Rev Cancer* (2014) 14(2):121–34. doi: 10.1038/nrc3647
- Cao ZQ, Wang Z, Leng P. Aberrant n-cadherin expression in cancer. *BioMed Pharmacother* (2019) 118:109320. doi: 10.1016/j.biopha.2019.109320
- Blaschuk OW. N-cadherin antagonists as oncology therapeutics. *Philos Trans R Soc Lond B Biol Sci* (2015) 370(1661):20140039. doi: 10.1098/rstb.2014.0039
- Meng X, Zhou A, Huang Y, Zhang Y, Xu Y, Shao K, et al. N-cadherin nanoantagonist driven mesenchymal-to-Epithelial transition in fibroblasts for improving reprogramming efficiency. *Nano Lett* (2021) 21(13):5540–6. doi: 10.1021/acs.nanolett.1c00880
- Gerhardt H, Wolburg H, Redies C. N-cadherin mediates pericytic-endothelial interaction during brain angiogenesis in the chicken. *Dev Dyn* (2000) 218(3):472–9. doi: 10.1002/1097-0177(200007)218:3<472::AID-DVDY1008>3.0.CO;2-
- Tanaka H, Kono E, Tran CP, Miyazaki H, Yamashiro J, Shimomura T, et al. Monoclonal antibody targeting of n-cadherin inhibits prostate cancer growth, metastasis and castration resistance. *Nat Med* (2010) 16(12):1414–20. doi: 10.1038/nm.2236
- Mrozik KM, Blaschuk OW, Cheong CM, Zannettino ACW, Vandyke K. N-cadherin in cancer metastasis, its emerging role in hematological malignancies and potential as a therapeutic target in cancer. *BMC Cancer* (2018) 18(1):939. doi: 10.1186/s12885-018-4845-0
- Yu W, Yang L, Li T, Zhang Y. Cadherin signaling in cancer: Its functions and role as a therapeutic target. *Front Oncol* (2019) 9:989. doi: 10.3389/fonc.2019.00989
- Perotti A, Sessa C, Mancuso A, Noverasco C, Cresta S, Locatelli A, et al. Clinical and pharmacological phase I evaluation of exherin (ADH-1), a selective anti-n-cadherin peptide in patients with n-cadherin-expressing solid tumors. *Ann Oncol* (2009) 20(4):741–5. doi: 10.1093/annonc/mdn695
- Shintani Y, Fukumoto Y, Chaika N, Grandgenett PM, Hollingsworth MA, Wheelock MJ, et al. ADH-1 suppresses n-cadherin-dependent pancreatic cancer progression. *Int J Cancer* (2008) 122(1):71–7. doi: 10.1002/ijc.23027
- Williams E, Williams G, Gour BJ, Blaschuk OW, Doherty P. A novel family of cyclic peptide antagonists suggests that n-cadherin specificity is determined by amino acids that flank the HAV motif. *J Biol Chem* (2000) 275(6):4007–12. doi: 10.1074/jbc.275.6.4007
- Islami M, Nezat F, Khajeh S, Mostafavi-Pour Z, Bagheri Novir S, Negahdaripour M, et al. Deep analysis of n-cadherin/ADH-1 interaction: A computational survey. *J Biomol Struct Dyn* (2019) 37(1):210–28. doi: 10.1080/07391102.2018.1424035
- Yarom N, Stewart D, Avruh L, Malik R, Wells J, Jonker DJ. ADH-1 in the treatment of metastatic adrenocortical carcinoma—case report. *Anticancer Res* (2011) 31(11):3921–5.
- Mariotti A, Perotti A, Sessa C, Rügge C. N-cadherin as a therapeutic target in cancer. *Expert Opin Investig Drugs* (2007) 16(4):451–65. doi: 10.1517/13543784.16.4.451
- Augustine CK, Yoshimoto Y, Gupta M, Zipfel PA, Selim MA, Febbo P, et al. Targeting n-cadherin enhances antitumor activity of cytotoxic therapies in melanoma treatment. *Cancer Res* (2008) 68(10):3777–84. doi: 10.1158/0008-5472.CAN-07-5949
- Beasley GM, Riboh JC, Augustine CK, Zager JS, Hochwald SN, Grobmyer SR, et al. Prospective multicenter phase II trial of systemic ADH-1 in combination with melphalan via isolated limb infusion in patients with advanced extremity melanoma. *J Clin Oncol* (2011) 29(9):1210–5. doi: 10.1200/JCO.2010.32.1224
- Kumar K, Ghosh A. 18F-ALF labeled peptide and protein conjugates as positron emission tomography imaging pharmaceuticals. *Bioconjug Chem* (2018) 29(4):953–75. doi: 10.1021/acs.bioconjugchem.7b00817
- Behrendt R, White P, Offer J. Advances in fmoc solid-phase peptide synthesis. *J Pept Sci* (2016) 22(1):4–27. doi: 10.1002/psc.2836
- McBride WJ, Sharkey RM, Karacay H, D'Souza CA, Rossi EA, Laverman P, et al. A novel method of 18F radiolabeling for PET. *J Nucl Med* (2009) 50(6):991–8. doi: 10.2967/jnumed.108.060418
- Tshibangu T, Cawthorne C, Serdons K, Pauwels E, Gsell W, Bormans G, et al. Automated GMP compliant production of [18F]ALF-NOTA-octreotide. *EJNMMI Radiopharm Chem* (2020) 5(1):4. doi: 10.1186/s41181-019-0084-1
- McBride WJ, D'Souza CA, Sharkey RM, Karacay H, Rossi EA, Chang CH, et al. Improved 18F labeling of peptides with a fluoride-aluminum-chelate complex. *Bioconjug Chem* (2010) 21(7):1331–40. doi: 10.1021/bc100137x
- Lang L, Li W, Guo N, Ma Y, Zhu L, Kiesewetter DO, et al. Comparison study of [18F]FAI-NOTA-PRGD2, [18F]FPPRGD2, and [68Ga]Ga-NOTA-PRGD2 for PET imaging of U87MG tumors in mice. *Bioconjug Chem* (2011) 22(12):2415–22. doi: 10.1021/bc200197h
- Liu S, Liu H, Jiang H, Xu Y, Zhang H, Cheng Z. One-step radiosynthesis of ¹⁸F-ALF-NOTA-RGD₂ for tumor angiogenesis PET imaging. *Eur J Nucl Med Mol Imaging* (2011) 38(9):1732–41. doi: 10.1007/s00259-011-1847-4
- Howard EW, Camm KD, Wong YC, Wang XH. E-cadherin upregulation as a therapeutic goal in cancer treatment. *Mini Rev Med Chem* (2008) 8(5):496–518. doi: 10.2174/138955708784223521
- Shih W, Yamada S. N-cadherin-mediated cell-cell adhesion promotes cell migration in a three-dimensional matrix. *J Cell Sci* (2012) 125(Pt 15):3661–70. doi: 10.1242/jcs.103861
- Shash LS, Ibrahim RA, Elgohary SA. E-cadherin and n-cadherin immunohistochemical expression in proliferating urothelial lesions: Potential novel cancer predictive EMT profiles. *Appl Immunohistochem Mol Morphol* (2021) 29(9):657–66. doi: 10.1097/PAL.0000000000000940
- Qian X, Anzovino A, Kim S, Suyama K, Yao J, Hulit J, et al. N-cadherin/FGFR promotes metastasis through epithelial-to-mesenchymal transition and stem/progenitor cell-like properties. *Oncogene* (2014) 33(26):3411–21. doi: 10.1038/nc.2013.310
- Hsu CC, Huang SF, Wang JS, Chu WK, Nien JE, Chen WS, et al. Interplay of n-cadherin and matrix metalloproteinase 9 enhances human nasopharyngeal carcinoma cell invasion. *BMC Cancer* (2016) 16(1):800. doi: 10.1186/s12885-016-2846-4
- Gouin KH3rd, Ing N, Plummer JT, Rosser CJ, Ben Cheikh B, Oh C, et al. An n-cadherin 2 expressing epithelial cell subpopulation predicts response to surgery, chemotherapy and immunotherapy in bladder cancer. *Nat Commun* (2021) 12(1):4906. doi: 10.1038/s41467-021-25103-7
- Elie-Caille C, Lascombe I, Pêchery A, Bittard H, Fauconnet S. Molecular and nanoscale evaluation of n-cadherin expression in invasive bladder cancer cells under control conditions or GW501516 exposure. *Mol Cell Biochem* (2020) 471(1-2):113–27. doi: 10.1007/s11010-020-03771-1
- Amschler K, Beyazpinar I, Erpenbeck L, Kruss S, Spatz JP, Schön MP. Morphological plasticity of human melanoma cells is determined by nanoscopic patterns of e- and n-cadherin interactions. *J Invest Dermatol* (2019) 139(3):562–72. doi: 10.1016/j.jid.2018.09.027
- Labernadie A, Kato T, Brugués A, Serra-Picamal X, Derzi S, Arwert E, et al. A mechanically active heterotypic e-cadherin/N-cadherin adhesion enables fibroblasts to drive cancer cell invasion. *Nat Cell Biol* (2017) 19(3):224–37. doi: 10.1038/ncb3478
- Tillet E, Vittet D, Féraud O, Moore R, Kemler R, Huber P. N-cadherin deficiency impairs pericyte recruitment, and not endothelial differentiation or sprouting, in embryonic stem cell-derived angiogenesis. *Exp Cell Res* (2005) 310(2):392–400. doi: 10.1016/j.yexcr.2005.08.021
- Blaschuk OW. Potential therapeutic applications of n-cadherin antagonists and agonists. *Front Cell Dev Biol* (2022) 10:866200. doi: 10.3389/fcell.2022.866200
- McBride WJ, Sharkey RM, Goldenberg DM. Radiofluorination using aluminum-fluoride (Al18F). *EJNMMI Res* (2013) 3(1):36. doi: 10.1186/2191-219X-3-36
- Goldenberg DM, Sharkey RM, McBride WJ, Boerman OC. Al18F: A new standard for radiofluorination. *J Nucl Med* (2013) 54(7):1170. doi: 10.2967/jnumed.113.125245
- Fersing C, Bouhlef A, Cantelli C, Garrigue P, Lisowski V, Guillet B. A comprehensive review of non-covalent radiofluorination approaches using aluminum [18F]fluoride: Will [18F]ALF replace 68Ga for metal chelate labeling? *Molecules* (2019) 24(16):2866. doi: 10.3390/molecules24162866